A fully implicit, monolithic FEM Newton multigrid based solution approach for large strain poroelasticity

Stefan Turek and Abdulrahman Obaid
(Dated: October 25, 2013)

This short report, directed to Prof. Markert, introduces briefly a new FEM solution scheme that could work for large deformation problem without restriction to certain frequency range for the 1st time using some CFD techniques.

Keywords: Multi-grid solver, Porous media dynamics (PMD), Coupled problem, Implicit-monolithic solution, Finite Element Method (FEM), Computational fluid dynamics (CFD).

1. THE OLD $\mathbf{uv}p$ - FORM

Proceeding from inviscid, convectionless fluid assumption, the $\mathbf{uv}p$ - form is the following governing set of partial differential equations

$$\rho^S (\mathbf{v}_S)'_S = \operatorname{div} \mathbf{T}^S_E - n^S \operatorname{grad} p + \rho^S \mathbf{b} + \frac{(n^F)^2 \gamma^{FR}}{k^F} (\mathbf{v}_F - \mathbf{v}_S) \tag{1}$$

$$\rho^F (\mathbf{v}_F)'_S + \cancel{\rho^F (\operatorname{grad} \mathbf{v}_F)(\mathbf{v}_F - \mathbf{v}_S)} = -n^F \operatorname{grad} p + \rho^F \mathbf{b} - \frac{(n^F)^2 \gamma^{FR}}{k^F} (\mathbf{v}_F - \mathbf{v}_S) \tag{2}$$

$$\operatorname{div} (n^F \mathbf{v}_F) + \operatorname{div} (n^S \mathbf{v}_S) = 0 \tag{3}$$

corresponding to the subsequent weak form:

$$\begin{aligned} &\int_\Omega \operatorname{grad} \delta\mathbf{u}_S : \mathbf{T}^S_E \, \mathrm{d}v - \int_\Omega n^S \operatorname{div} \delta\mathbf{u}_S \, p \, \mathrm{d}v - \int_\Omega \frac{(n^F)^2 \gamma^{FR}}{k^F} \delta\mathbf{u}_S \cdot (\mathbf{v}_F - \mathbf{v}_S) \, \mathrm{d}v \\ &+ \int_\Omega \rho^S \delta\mathbf{u}_S \cdot \left\{ (\mathbf{v}_S)'_S - \mathbf{b} \right\} \mathrm{d}v - \int_\Omega p \, \delta\mathbf{u}_S \cdot \underline{\operatorname{grad} n^S} \, \mathrm{d}v = \int_{\Gamma_{\mathbf{t}^S}} \delta\mathbf{u}_S \cdot \bar{\mathbf{t}}^S \, \mathrm{d}a \end{aligned} \tag{4}$$

$$\begin{aligned} &- \int_\Omega n^F \operatorname{div} \delta\mathbf{v}_F \, p \, \mathrm{d}v + \int_\Omega \frac{(n^F)^2 \gamma^{FR}}{k^F} \delta\mathbf{v}_F \cdot (\mathbf{v}_F - \mathbf{v}_S) \, \mathrm{d}v + \int_\Omega \rho^F \delta\mathbf{v}_F \cdot \left\{ (\mathbf{v}_F)'_S - \mathbf{b} \right\} \mathrm{d}v \\ &- \int_\Omega p \, \delta\mathbf{w} \cdot \underline{\operatorname{grad} n^F} \, \mathrm{d}v = \int_{\Gamma_{\mathbf{t}^F}} \delta\mathbf{v}_F \cdot \bar{\mathbf{t}}^F \, \mathrm{d}a \end{aligned} \tag{5}$$

$$\int_\Omega \delta p \, \underline{\operatorname{div} (n^S \mathbf{v}_S)} \, \mathrm{d}v + \int_\Omega n^F \delta p \, \underline{\operatorname{div} (n^F \mathbf{v}_F)} \, \mathrm{d}v = 0 \tag{6}$$

$$\int_\Omega \delta\mathbf{u}_S \cdot \left\{ (\mathbf{u}_S)'_S - \mathbf{v}_S \right\} \mathrm{d}v = 0 \, . \tag{7}$$

Where the underlined terms include second derivatives and hence lower order elements CANNOT be used here. **This a disadvantage that can be eliminated in the new $\mathrm{uw}p$(2)-form, introduced in the subsequent section. Beside that, This weak form does not allow for the direct use of CFD techniques in case of large deformation which is also overcome in the following section**. The boundary $\Gamma = \partial\Omega$ is divided into Dirichlet (essential) and Neumann (natural) boundaries, respectively, resulting in $\Gamma = \Gamma_{\mathbf{u}_S} \cup \Gamma_{\mathbf{t}^S}$ for the balance of momentum of the solid phase and in $\Gamma = \Gamma_{\mathbf{v}_F} \cup \Gamma_{\mathbf{t}^F}$ for the balance of momentum of the fluid phase, wherein the tractions are defined as

$$\bar{\mathbf{t}}^S = \left(\mathbf{T}^S_E - n^S p \mathbf{I} \right) \cdot \mathbf{n} \, , \qquad \bar{\mathbf{t}}^F = -n^F p \mathbf{n} \, . \tag{8}$$

Remark that $\bar{\mathbf{t}}^F$ is a function of $\mathbf{u}_S$ and p. Therefore, **knowing boundary pressure values is , in general, not enough to evaluate the fluid traction (exception: when $p = 0$). This also a disadvantage that is eliminated in the subsequent section**. To differentiate the special shape of the incompressibility condition in the weak form from the classical forms mentioned Table I in [2], this method is called $\mathbf{uv}p(3)$ and written in the following matrix-vector notation:

$$\mathbf{M}\dot{\mathbf{y}} + \mathbf{K}\mathbf{y} = \mathbf{f}\,. \tag{9}$$

Or in more detail with mass and stiffness matrices and right hand side vectors, one obtains with $\mathbf{y}^T = [\,\mathbf{u}_S^T\,\mathbf{v}_S^T\,\mathbf{v}_F^T\,p^T\,]$

$$\begin{pmatrix} \mathbf{M}_{\mathbf{v}_S\mathbf{u}_S} & \mathbf{0} & \mathbf{0} & \mathbf{0} \\ \mathbf{0} & \mathbf{M}_{\mathbf{u}_S\mathbf{v}_S} & \mathbf{0} & \mathbf{0} \\ \mathbf{0} & \mathbf{0} & \mathbf{M}_{\mathbf{v}_F\mathbf{v}_F} & \mathbf{0} \\ \mathbf{0} & \mathbf{0} & \mathbf{0} & 0 \end{pmatrix} \begin{pmatrix} \dot{\mathbf{u}}_S \\ \dot{\mathbf{v}}_S \\ \dot{\mathbf{v}}_F \\ \dot{p} \end{pmatrix} + \begin{pmatrix} \mathbf{0} & \mathbf{K}_{\mathbf{v}_S\mathbf{v}_S} & \mathbf{0} & \mathbf{0} \\ \mathbf{K}_{\mathbf{u}_S\mathbf{u}_S} & \mathbf{K}_{\mathbf{u}_S\mathbf{v}_S} & \mathbf{K}_{\mathbf{u}_S\mathbf{v}_F} & \mathbf{K}_{\mathbf{u}_Sp} \\ \mathbf{0} & \mathbf{K}_{\mathbf{v}_F\mathbf{v}_S} & \mathbf{K}_{\mathbf{v}_F\mathbf{v}_F} & \mathbf{K}_{\mathbf{v}_Fp} \\ \mathbf{0} & \mathbf{K}_{p\mathbf{v}_S} & \mathbf{K}_{p\mathbf{v}_F} & 0 \end{pmatrix} \begin{pmatrix} \mathbf{u}_S \\ \mathbf{v}_S \\ \mathbf{v}_F \\ p \end{pmatrix} = \begin{pmatrix} \mathbf{0} \\ \mathbf{f}_{\mathbf{u}_S} + \mathbf{b}_S \\ \mathbf{f}_{\mathbf{v}_F} + \mathbf{b}_F \\ \mathbf{0} \end{pmatrix} \tag{10}$$

It remains to mention that this $\mathbf{uv}p$ allowed us to test the effect of the convective term and the fluid friction while adopting the small deformation assumption in the solid skeleton In less number of terms than the new $\mathbf{uw}p$ (2) form. As the both terms turned out to be negligible, $\mathbf{uw}p$ (2) - form is an excellent alternative. For detailed description of the $\mathbf{uv}p$ - form, please look at our joint paper [1].

2. THE NEW $\mathbf{uw}p$ - FORM

The old $\mathbf{uv}p$ approach appeared to be efficient in case of infinitesimal deformation where n^S and n^F can be considered as constant values, they do not allow for the direct implementation of CFD techniques in the case of large deformation when using Q2/P1 element due to the arising of $\operatorname{grad} n^S$ and $\operatorname{grad} n^F$ in (4) and (5) when conducting integration by parts (essential to avoid having the differential operator 'grad $(\cdot)$' acting on the discontinuous pressure element P1) and in (6) since $\operatorname{div} n^F\mathbf{v}_F = \operatorname{grad} n^F\cdot\mathbf{v}_F + n^F\operatorname{div}\mathbf{v}_F$ and $\operatorname{div} n^S\mathbf{v}_S = \operatorname{grad} n^S\cdot\mathbf{v}_S + n^S\operatorname{div}\mathbf{v}_S$. We dislike these terms as we seek to write our non-linear problem in the nice form of (29) , similar to Stokes or Navier-Stokes form, where $\mathbf{B}$ and $\mathbf{B}^T$ represents only the grad operaotr and the div operator respectively so that we can use the CFD techniques, originally designed to solve the non-linear Navier-Stokes equation. To overcome this problem, we write (1)-(3) in term of flow velocity $\mathbf{w}$, i.e., we set

$$\mathbf{w} = n^F(\mathbf{v}_F - \mathbf{v}_S) \quad \rightarrow \quad \mathbf{v}_F = \frac{\mathbf{w}}{n^F} + \mathbf{v}_S \tag{11}$$

Substitution of (11) in the left hand side of (2), we get that

$$\rho^F(\mathbf{v}_F)'_S + \rho^F(\operatorname{grad}\mathbf{v}_F)(\mathbf{v}_F - \mathbf{v}_S) = \rho^F\left[\frac{\mathbf{w}}{n^F} + \mathbf{v}_S\right]'_S + \cancel{\rho^F \operatorname{grad}\left[\frac{\mathbf{w}}{n^F} + \mathbf{v}_S\right]\left[\frac{\mathbf{w}}{n^F}\right]} \tag{12}$$

$$= \rho^F\left[\frac{n^F(\mathbf{w})'_S - \mathbf{w}\cdot(n^F)'_S}{(n^F)^2} + (\mathbf{v}_S)'_S\right] = \rho^{FR}\left[(\mathbf{w})'_S + \mathbf{w}\cdot\operatorname{div}\mathbf{v}_S + n^F(\mathbf{v}_S)'_S\right]$$

Remark that we have used the useful relation:

$$(n^F)'_S + n^F\operatorname{div}\mathbf{v}_S = 0 \tag{13}$$

the orange nonlinear convective term is omitted by magnitude argument. Notice that if n^F is constant, then the time derivative $(n^F)'_S$ is equal to zero and according to (13), the green term $\mathbf{w}\cdot\operatorname{div}\mathbf{v}_S$ is zero. Next, substitution of (11) and (12) in (1)-(3) and after some arrangements, we get the so-called $\mathbf{uw}p$-form:

$$\left[\rho^S + \rho^F\right](\mathbf{v}_S)'_S + \rho^{FR}(\mathbf{w})'_S - \operatorname{div}\mathbf{T}^S_E + \operatorname{grad} p + \rho^{FR}\mathbf{w}\cdot\operatorname{div}\mathbf{v}_S = \left[\rho^S + \rho^F\right]\mathbf{b} \tag{14}$$

$$\rho^{FR}(\mathbf{v}_S)'_S + \frac{\rho^{FR}}{n^F}(\mathbf{w})'_S + \frac{\rho^{FR}}{n^F}\mathbf{w}\cdot\operatorname{div}\mathbf{v}_S + \operatorname{grad} p + \frac{\gamma^{FR}}{k^F}\mathbf{w} = \rho^{FR}\mathbf{b} \tag{15}$$

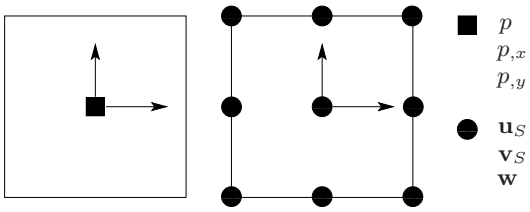

FIG. 1: The discontinuous linear pressure element P1 (left) and the 9-node Lagrange biquadratic element Q2 (right) that are used for the $\mathbf{uw}p(2)$-TR method.

$$\operatorname{div}\mathbf{w} + \operatorname{div}\mathbf{v}_S = 0 \tag{16}$$

$$(\mathbf{u}_S)'_S = \mathbf{v}_S\,, \tag{17}$$

Here (14) is the mixture momentum balance resulting from adding up the two balances of momentum.

3. WEAK FORMULATION AND DISCRETIZATION IN SPACE AND TIME

Our subsequent variational form of the $\mathbf{uw}p$ approach is created by multiplying (14)-(16) with the displacement test function $\delta\mathbf{u}_S$, the flow velocity test function $\delta\mathbf{w}$, the pressure test function δp, integrating over the whole domain Ω and performing partial integrations. Finally, we obtain the following weak form:

$$\begin{aligned}&\int_\Omega \operatorname{grad}\delta\mathbf{u}_S : \mathbf{T}^S_E \,\mathrm{d}v - \int_\Omega \operatorname{div}\delta\mathbf{u}_S\, p\,\mathrm{d}v + \int_\Omega \left[\rho^S + \rho^F\right]\delta\mathbf{u}_S\cdot(\mathbf{v}_S)'_S\,\mathrm{d}v \\ &+ \int_\Omega \rho^{FR}\delta\mathbf{u}_S\cdot[(\mathbf{w})'_S + \mathbf{w}\cdot\operatorname{div}\mathbf{v}_S]\,\mathrm{d}v \quad = \int_\Omega \left[\rho^S + \rho^F\right]\delta\mathbf{u}_S\cdot\mathbf{b}\,\mathrm{d}v + \int_{\Gamma_{\mathbf{t}^S}}\delta\mathbf{u}_S\cdot\bar{\mathbf{t}}^S\,\mathrm{d}a\end{aligned} \tag{18}$$

$$\begin{aligned}&\int_\Omega \frac{\gamma^{FR}}{k^F}\,\delta\mathbf{w}\cdot\mathbf{w}\,\mathrm{d}v - \int_\Omega \operatorname{div}\delta\mathbf{w}\, p\,\mathrm{d}v + \int_\Omega \frac{\rho^{FR}}{n^F}\delta\mathbf{w}\cdot[\mathbf{w}\cdot\operatorname{div}\mathbf{v}_S + (\mathbf{w})'_S]\,\mathrm{d}v \\ &+ \int_\Omega \rho^{FR}\delta\mathbf{w}\cdot(\mathbf{v}_S)'_S\,\mathrm{d}v \quad = \int_\Omega \rho^{FR}\delta\mathbf{w}\cdot\mathbf{b}\,\mathrm{d}v + \int_{\Gamma_{\mathbf{t}^F}}\delta\mathbf{w}\cdot\bar{\mathbf{t}}^F\,\mathrm{d}a\end{aligned} \tag{19}$$

$$\int_\Omega \delta p\,\operatorname{div}\mathbf{v}_S\,\mathrm{d}v + \int_\Omega \delta p\,\operatorname{div}\mathbf{w}\,\mathrm{d}v = 0 \tag{20}$$

Finally, we multiply (17) with the solid velocity test function $\delta\mathbf{v}_S$ and integrate over Ω:

$$\int_\Omega \delta\mathbf{v}_S\cdot[(\mathbf{u}_S)'_S - \mathbf{v}_S]\,\mathrm{d}v = 0\,. \tag{21}$$

As the above convectionless weak form requires weaker derivative than the convectionless $\mathbf{uv}p$-form, lower order elements can be used. The boundary $\Gamma = \partial\Omega$ is divided into Dirichlet (essential) and Neumann (natural) boundaries, respectively, resulting in $\Gamma = \Gamma_{\mathbf{u}_S}\cup\Gamma_{\mathbf{t}^S}$ for the balance of momentum of the solid phase and in $\Gamma = \Gamma_{\mathbf{w}}\cup\Gamma_{\mathbf{t}^F}$ for the balance of momentum of the fluid phase, wherein the tractions are defined as

$$\bar{\mathbf{t}}^S = \left(\mathbf{T}^S_E - p\mathbf{I}\right)\cdot\mathbf{n}\,, \qquad\qquad \bar{\mathbf{t}}^F = -p\mathbf{n}\,. \tag{22}$$

Observe that $\bar{\mathbf{t}}^F$ is now a function of only boundary pressures and hence it is easy to deal with in case of large deformation We shall adopt the fully implicit time integrator that is already discussed in our joint paper [1]. We will also use the Q2/P1 element pair, depicted in Figure 1, and the special multigrid solver introduced there. Based on the

discretization with the introduced FEM spaces, equations (18)-(21) can be written in the following matrix-vector notation:

$$\mathbf{M}\dot{\mathbf{y}} + \mathbf{K}\mathbf{y} = \mathbf{f}\,. \tag{23}$$

In more detail with mass and stiffness matrices and right hand side vectors, one obtains with $\mathbf{y}^T = [\,\mathbf{u}_S^T\,\mathbf{v}_S^T\,\mathbf{w}^T\,p^T\,]$

$$\begin{pmatrix} \mathbf{M_{vu}} & \mathbf{0} & \mathbf{0} & \mathbf{0} \\ \mathbf{0} & \mathbf{M_{uv}} & \mathbf{M_{uw}} & \mathbf{0} \\ \mathbf{0} & \mathbf{M_{wv}} & \mathbf{M_{ww}} & \mathbf{0} \\ \mathbf{0} & \mathbf{0} & \mathbf{0} & \mathbf{0} \end{pmatrix} \begin{pmatrix} \dot{\mathbf{u}}_S \\ \dot{\mathbf{v}}_S \\ \dot{\mathbf{w}} \\ \dot{p} \end{pmatrix} + \begin{pmatrix} \mathbf{0} & \mathbf{K_{vv}} & \mathbf{0} & \mathbf{0} \\ \mathbf{K_{uu}} & \mathbf{0} & \mathbf{K_{uw}} & \mathbf{K_{up}} \\ \mathbf{0} & \mathbf{0} & \mathbf{K_{ww}} & \mathbf{K_{wp}} \\ \mathbf{0} & \mathbf{K}_{pv} & \mathbf{K}_{pw} & \mathbf{0} \end{pmatrix} \begin{pmatrix} \mathbf{u}_S \\ \mathbf{v}_S \\ \mathbf{w} \\ p \end{pmatrix} = \begin{pmatrix} \mathbf{f_u} + \mathbf{b}_u \\ \mathbf{0} \\ \mathbf{f_w} + \mathbf{b}_w \\ \mathbf{0} \end{pmatrix} \tag{24}$$

with the following matrices and right hand side vectors:

$$\begin{aligned}
&\mathbf{K_{uu}} = \int_\Omega \operatorname{grad}\delta\mathbf{u}_S \colon \mathbf{T}_E^S \,\mathrm{d}v, \qquad \mathbf{K_{uw}} = \int_\Omega \delta\mathbf{u}_S \cdot \mathbf{w} \cdot \operatorname{div}\mathbf{v}_S \,\mathrm{d}v \\
&\mathbf{K_{up}} = -\int_\Omega \operatorname{div}\delta\mathbf{u}_S \, p \,\mathrm{d}v, \qquad \mathbf{K_{vv}} = -\int_\Omega \delta\mathbf{v}_S \cdot \mathbf{v}_S \,\mathrm{d}v \\
&\hat{\mathbf{K}}_{\mathbf{ww}} = \int_\Omega \frac{\gamma^{FR}}{k^F}\,\delta\mathbf{w}\cdot\mathbf{w}\,\mathrm{d}v, \qquad \tilde{\mathbf{K}}_{\mathbf{ww}} = \int_\Omega \frac{\rho^{FR}}{n^F}\delta\mathbf{w}\cdot\mathbf{w}\cdot\operatorname{div}\mathbf{v}_S\,\mathrm{d}v, \qquad \mathbf{K_{ww}} = \tilde{\mathbf{K}}_{\mathbf{ww}} + \hat{\mathbf{K}}_{\mathbf{ww}} \\
&\mathbf{K_{wp}} = -\int_\Omega \operatorname{div}\delta\mathbf{w}\, p\,\mathrm{d}v, \qquad \mathbf{K}_{pv} = \int_\Omega \delta p \operatorname{div}\mathbf{v}_S\,\mathrm{d}v, \qquad \mathbf{K}_{pw} = \int_\Omega \delta p \operatorname{div}\mathbf{w}\,\mathrm{d}v \\
&\mathbf{M_{uv}} = \int_\Omega \left[\rho^S + \rho^F\right]\delta\mathbf{u}_S\cdot(\mathbf{v}_S)'_S\,\mathrm{d}v, \qquad \mathbf{M_{vu}} = \int_\Omega \delta\mathbf{v}_S\cdot(\mathbf{u}_S)'_S\,\mathrm{d}v \\
&\mathbf{M_{uw}} = \int_\Omega \rho^{FR}\delta\mathbf{u}_S\cdot(\mathbf{w})'_S\,\mathrm{d}v, \qquad \mathbf{M_{wv}} = \int_\Omega \rho^{FR}\delta\mathbf{w}\cdot(\mathbf{v}_S)'_S\,\mathrm{d}v, \qquad \mathbf{M_{ww}} = \int_\Omega \frac{\rho^{FR}}{n^F}\delta\mathbf{w}\cdot(\mathbf{w})'_S\,\mathrm{d}v \\
&\mathbf{f_u} = \int_{\Gamma_{\mathbf{t}^S}} \delta\mathbf{u}_S\cdot\bar{\mathbf{t}}^S\,\mathrm{d}a + \int_\Omega \left[\rho^S+\rho^F\right]\delta\mathbf{u}_S\cdot\mathbf{b}\,\mathrm{d}v, \qquad \mathbf{f_w} = \int_{\Gamma_{\mathbf{t}^F}} \delta\mathbf{w}\cdot\bar{\mathbf{t}}^F\,\mathrm{d}a + \int_\Omega \rho^{FR}\delta\mathbf{w}\cdot\mathbf{b}\,\mathrm{d}v \\
&\mathbf{b_u} = \int_\Omega \left[\rho^S+\rho^F\right]\delta\mathbf{u}_S\cdot\mathbf{b}\,\mathrm{d}v, \qquad \mathbf{b_w} = \int_\Omega \rho^{FR}\delta\mathbf{w}\cdot\mathbf{b}\,\mathrm{d}v
\end{aligned} \tag{25}$$

Where the two green terms are to be neglected for infinitesimal deformation. In the next step, regarding the time integration, equations, we adopt the time integrator presented in [1] in which (23) or (24) are treated in a monolithic implicit way leading to a fully coupled system. In our approach, we apply the standard one-step θ-scheme to these systems, leading to

$$\mathbf{M}\frac{\mathbf{y}_{n+1}-\mathbf{y}_n}{\Delta t} + \theta\mathbf{K}\mathbf{y}_{n+1} = -\,(1-\theta)\,\mathbf{K}\mathbf{y}_n + \theta\mathbf{f}_{n+1} + (1-\theta)\mathbf{f}_n\,. \tag{26}$$

However, as an important remark for the subsequent more detailed description, the red-colored continuity equation due to the incompressibility constraint and the blue-colored pressure p as corresponding Lagrange multiplier are always treated fully implicitly (that means, as usual in CFD simulations, $\theta = 1$), which leads to second-order accuracy (cf. [5]).

$$\begin{pmatrix} \mathbf{M_{vu}} & \theta_1\mathbf{K_{vv}} & \mathbf{0} & \mathbf{0} \\ \theta_1\mathbf{K_{uu}} & \mathbf{M_{uv}} & \mathbf{M_{uw}}+\theta_1\mathbf{K_{uw}} & \mathbf{K_{up}} \\ 0 & \mathbf{M_{wv}} & \mathbf{M_{ww}}+\theta_1\mathbf{K_{ww}} & \mathbf{K_{wp}} \\ 0 & \mathbf{K_{pv}} & \mathbf{K_{pw}} & \mathbf{0} \end{pmatrix} \begin{pmatrix} \mathbf{u}_S \\ \mathbf{v}_S \\ \mathbf{w} \\ \overline{p} \end{pmatrix}_{n+1} = \begin{pmatrix} \mathbf{M_{vu}} & \theta_2\mathbf{K_{vv}} & \mathbf{0} & \mathbf{0} \\ \theta_2\mathbf{K_{uu}} & \mathbf{M_{uv}} & \mathbf{M_{uw}}+\theta_2\mathbf{K_{uw}} & \mathbf{0} \\ 0 & \mathbf{M_{wv}} & \mathbf{M_{ww}}+\theta_2\mathbf{K_{ww}} & \mathbf{0} \\ 0 & \mathbf{0} & \mathbf{0} & \mathbf{0} \end{pmatrix} \begin{pmatrix} \mathbf{u}_S \\ \mathbf{v}_S \\ \mathbf{w} \\ \overline{p} \end{pmatrix}_n + \theta_1\mathbf{f}_{n+1} - \theta_2\mathbf{f}_n \tag{27}$$

with

$$\theta_1 = \theta\Delta t\,, \quad \theta_2 = (\theta-1)\Delta t \tag{28}$$

Note that the time steps (Δt), supposed to be in front of the (blue) pressure matrices, are absorbed into $\overline{p} = \Delta t\, p$, as usually done in CFD, leading to the following saddle-point problem with $\mathbf{U}^T = [\,\mathbf{u}_S^T\, \mathbf{v}_S^T\, \mathbf{w}^T\,]$ that we solve for every time step:

$$\begin{pmatrix} \tilde{\mathbf{A}} & \mathbf{B} \\ \mathbf{B}^{\mathrm{T}} & \mathbf{0} \end{pmatrix} \begin{pmatrix} \mathbf{U} \\ \overline{p} \end{pmatrix} = \begin{pmatrix} \mathbf{rhs\ U} \\ \mathbf{rhs\ p} \end{pmatrix} \tag{29}$$

After solving the above non-linear saddle-point system with FEAT special CFD solver, the pressure is scaled back using the relation $p = \overline{p}/\Delta t$. Setting $\theta = 1/2$, we recover the second-order Crank-Nicolson scheme (in time), which is based on the well-known trapezoidal rule (TR).

4. NUMERICAL VALIDATION

To validate and to evaluate our discussed formulations (which all have been realized in our in-house code FEATFLOW [6]), we shall compare our calculations with the highly accurate **uv**p(3)-TR-Q2/P1 technique, discussed in [1]. Therefore, the three numerical examples , already solved in [1], are solved again but with our new **uw**p(2)-TR-Q2/P1 approach which stands for the described monolithic solver for the **uw**p formulation based on the weak forms (18)-(21) using the fully implicit Crank-Nicolson ($\theta = 1/2$) time integration scheme as shown in (27) and the mixed finite element pairs Q2/P1 shown in Figure 1. The number 2 in **uw**p(2)-TR-Q2/P1 is used to distinguish our solution algorithms from those in Table I in [2].

4.1. Results I: Saturated poroelastic column under harmonic load

In this example, a rectangular domain of a homogeneous, isotropic and water-saturated poroelastic medium is subjected at the perfectly drained ($\bar{\mathbf{t}}^F = \mathbf{0}$) top to a compressive sinusoidal load, defined by

$$f(t) = 10^3[\,1 - \cos(20\,\pi\,t)\,]\ \ [\mathrm{N/m^2}]\,,$$

and at the bottom, left and right to impermeable, frictionless but rigid boundaries. Here, an infinitesimal linear elastic plane strain deformation is assumed and the geometry with boundary conditions and meshes are illustrated in Figure 2 and Table I.

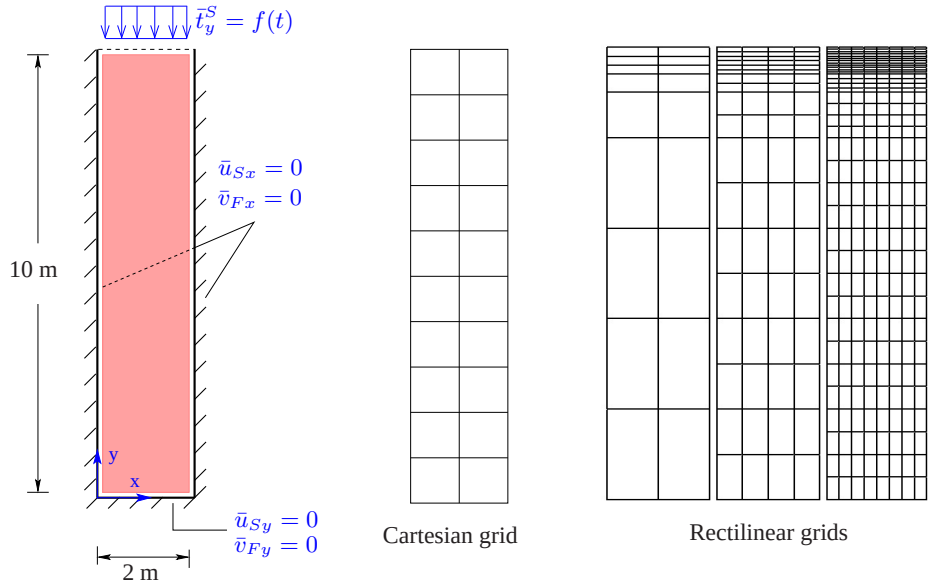

FIG. 2: Geometry and boundary conditions (left), Cartesian mesh: 1 element per meter (middle) and rectilinear mesh level 1, 2 & 3 (right). This figure is related to table I and Table II

TABLE I: Total number of elements and unknowns (five primary unknowns u_{Sx}, u_{Sy}, w_x, w_y and p plus two secondary unknowns v_{Sx} and v_{Sy}) for the $\mathbf{uw}p$(3)-TR-Q2/P1 approach. This table is related to the meshes in Figure 2.

Cartesian			Rectilinear		
#Elem./m	#Elem.	#Unknowns	Level	#Elem.	#Unknowns
1	20	690	1	18	625
5	500	14226	2	72	2214
10	2000	55446	3	288	8310
15	4500	123666	4	1152	32166
20	8000	218886	5	4608	126534
50	50000	1357206	-	-	-
100	200000	5414406	-	-	-

TABLE II: Physical properties of the porous medium used for all simulations.

Parameter	Symbol	Value	SI Unit
first Lamé constant of solid	μ^S	5.583×10^6	$\mathrm{N/m^2}$
second Lamé constant of solid	λ^S	8.375×10^6	$\mathrm{N/m^2}$
Effective density of dense solid	ρ^{SR}	2000	$\mathrm{kg/m^3}$
Effective density of pore fluid	ρ^{FR}	1000	$\mathrm{kg/m^3}$
Initial volume fraction of solid	$n^S = n^S_{0S}$	0.67	$-$
Darcy permeability	k^F	$10^{-2}, 10^{-5}$	$\mathrm{m/s}$

The first aim of this simple benchmark problem is to validate our monolithic $\mathbf{uw}p$(2)-TR-Q2/P1 approach by comparing its solutions with the reference solutions for the solid displacement and the pore-fluid pressure obtained by analytically solving a one-dimensional PDE.

The second aim is to compare quantitatively the accuracy of the new monolithic $\mathbf{uw}p$(2)-TR-Q2/P1 with the highly accurate $\mathbf{uv}p$(3)-TR-Q2/P1 presented in [1]. Therefore, The adopted constitutive material parameters (listed in Table II), are same as those in [1]. . As we are using an implicit time integrator which is unconditionally stable, our computations are performed on anisotropic meshes (see the rectilinear mesh in Figure 2) that get finer when approaching the top (perfect drainage) loaded boundary to capture the high pressure gradient that suddenly forms in a small layer below the boundary. From Figures 3 and 4, it follows that the described $\mathbf{uw}p$(2)-TR-Q2/P1 technique yields convergent approximations of the solid displacement and pressure field following the analytical reference solution.

Next, we compare the accuracy of our monolithic $\mathbf{uw}p$(2)-TR-Q2/P1 with the most accurate $\mathbf{uv}p$(3)-TR-Q2/P1. In this regard, we adopt the Cartesian mesh in stead of the preferred rectilinear one as the results reported in [1] are based on this discretization. From Figure 5 which shows non-fully converged solutions, we remark that the both techniques for this linear problem leads to identical accuracy as confirmed by 6 which is expected for such a linear problem as we used the same FEM elements, the same time integrator and the direct UMFPACK solver.

It worths to mention that the used piecewise discontinuous pressure element P1 has no pressures prescribed at the boundary and it should not. The boundary pressure values are interpreted as fluid tractions (see (8)) and if we compute the value of pressure at the top loaded boundary by interpolation we get a 'false' value (600 pa) with large error as shown in Figure 5 but in-spite of that, the relative error in the displacement at the top is much smaller. This indicates that at least a small error in the pressure at the loaded fully-drained boundary does not significantly influence the full convergence of the displacement. However, as the value of the pressure at the boundary is already given, it should not be computed by interpolation, but taken as it is and can be well approximated with the rectilinear mesh.

5. TWO-DIMENSIONAL WAVE PROPAGATION

The test is show almost identical solutions. Therefore the results are removed.

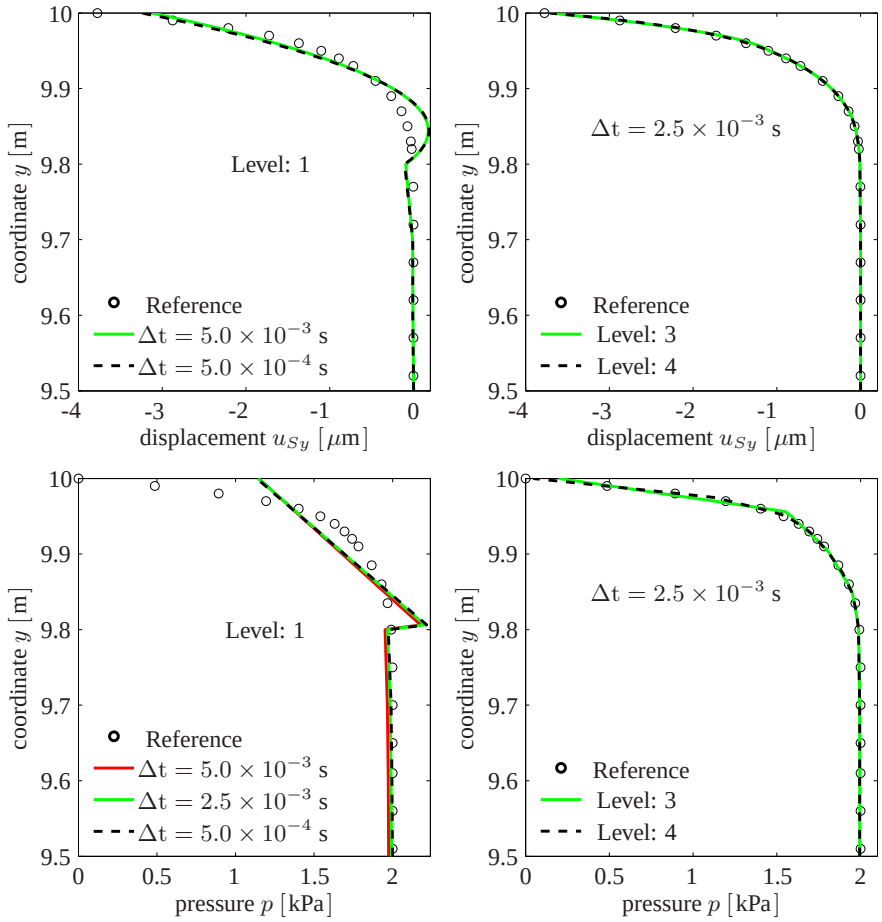

FIG. 3: Solid displacement distribution (top) and pressure distribution (bottom) in the first half meter under the loaded top of the column at time $= 0.15$ s using **uw**p(2)-TR-Q2/P1 for $k^F = 10^{-5}$ m/s and the rectilinear mesh (cf. Figure 2 right). The reference solution is taken from [2].

6. QUESTIONS TO PROF. MARKERT

We would like to solve the first configuration (see Figure 2), but for a rate-independent material model with large deformation. In particular, we seek to solve a hyper-elstic model suitable for TPM. As far as Obaid knows, there are several models that relates permeability and volume for incompressible material of solid skeleton

- A model that has been used to describe biological tissue: $f(J) = \exp(M(J-1))$
- Eipper model for totally compressed void spaces indeed prevents flow

$$\mathbf{T}^{\mathrm{S}}_{\mathrm{E}} = \frac{\mu^{\mathrm{S}}}{J_{\mathrm{S}}}(\mathbf{F}_{\mathrm{S}}\mathbf{F}_{\mathrm{S}} - \mathbf{I}) + \lambda^{\mathrm{S}}(1 - n^{\mathrm{S}}_0)\Big(\frac{1}{1 - n^{\mathrm{S}}_0} - \frac{1}{J_{\mathrm{S}} - n^{\mathrm{S}}_0}\Big)\mathbf{I}.$$

the model introduced by Gernot Eipper has a problem to describe certain phenomena in soil that was overcome by a new model introduce by Prof. Marker as Prof. Markert indicated in one of his old emails.

We need to have Prof. Markert's governing equation for the stress in term of the deformation gradient (and results latter) in a simple form that can be easily read by programmer. As we intend to use the updated Lagrangian formulation mixed with our CFD technique, we can use a special CFD non-linear solver that is fast enough without the need for linearization.

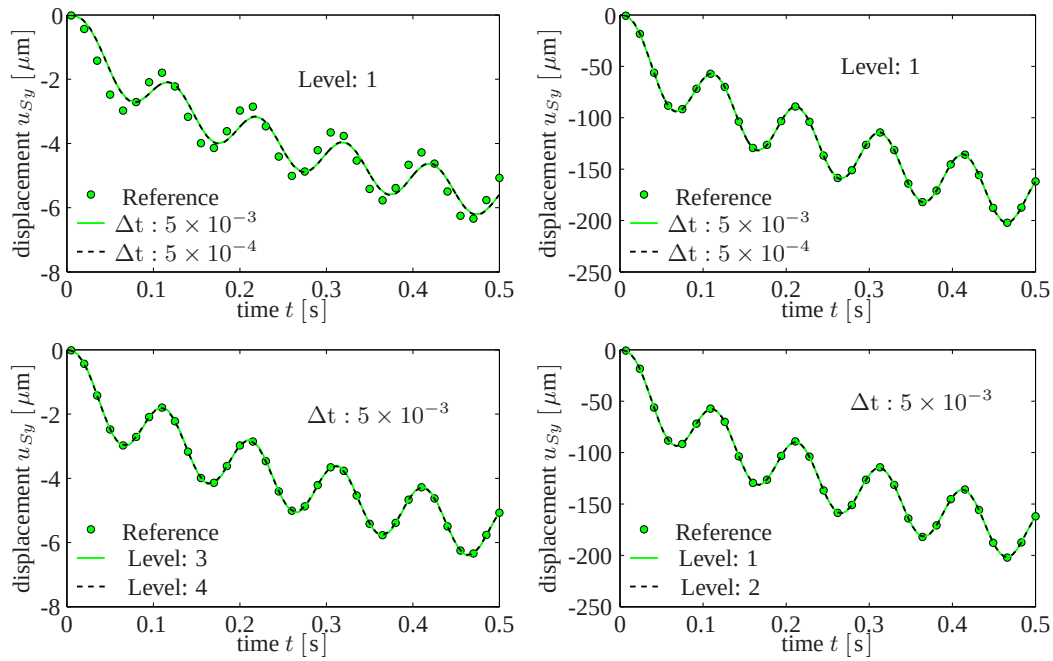

FIG. 4: y-displacement at point (1,10) vs. time using **uw**p(2)-TR-Q2/P1 for $k^F = 10^{-5}$m/s (left) and for $k^F = 10^{-2}$m/s (right) for rectilinear mesh (cf. Figure 2 right). The reference solution is taken from [2].

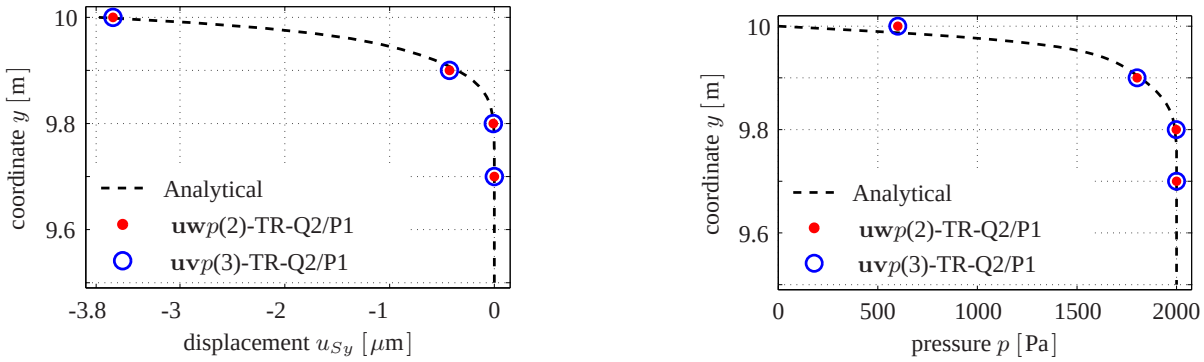

Height	Analytical solution	**uv**p(3)-TR-Q2/P1	**uw**p(2)-TR-Q2/P1	Absolute Error
9.7	-3.649199×10^{-5}	2.894931×10^{-4}	2.894931×10^{-4}	0.0003
9.8	-9.027950×10^{-3}	-1.035450×10^{-2}	-1.035450×10^{-2}	0.0010
9.9	-3.511237×10^{-1}	-4.279263×10^{-1}	-4.27926310^{-1}	0.077
10	-3.772775	-3.639146	-3.639146	0.13

Height	Analytical solution	**uv**p(3)-TR-Q2/P1	**uw**p(2)-TR-Q2/P1	Absolute Error
9.7	2000.0	2000.0	2000.0	0.0
9.8	1991.8	1997.7	1997.7	5.9
9.9	1818.5	1801.9	1801.9	16.6
10	0	~~600~~	~~600~~	~~600~~

FIG. 5: Non fully converged solid displacement and absolute errors in μm (left) and pore fluid pressure and absolute errors in pa (right) for the first half meter below the top surface for the isotropic Cartesian mesh (10 elem/m) (cf. Figure 2, center) for $k^F = 10^{-5}$m/s at $t = 0.15$ s. Analytical solutions are taken from [2].

once the non-linear solver work, we shall compare its efficiency with Newton method.

[1] S. Turek, A. Obaid, and B. Markert, Journal of Coupled Systems and Multiscale Dynamics (2013), accepted.
[2] B. Markert, Y. Heider, and W. Ehlers, Int. J. Numer. Meth. Eng. **82**, 1341 (2010).
[3] B. Markert, Transp. Porous Med. **70**, 427 (2007).

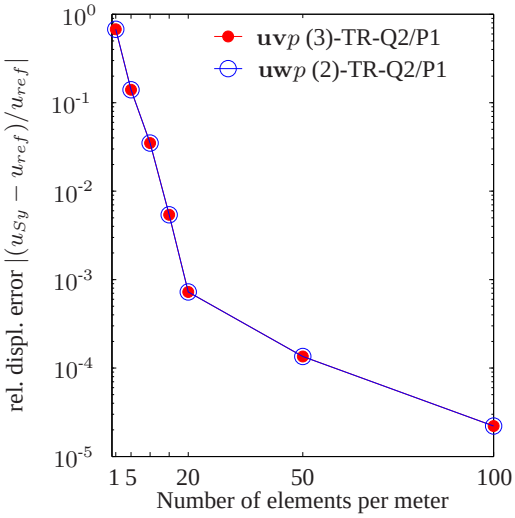

No. elem. per m	**uv**p(3)-TR-Q2/P1	**uw**p(2)-TR-Q2/P1	Relative errors
1	-1.219813005	-1.219813005	0.6767
5	-3.254548454	-3.254548454	0.14
10	-3.639145997	-3.639145997	0.035
15	-3.7523677745	-3.7523677745	0.00541
20	-3.7755129465	-3.7755129465	7.26×10^{-4}
50	-3.7732859810	-3.7732859810	1.35×10^{-4}
100	-3.772691556	-3.772691556	2.21×10^{-5}

FIG. 6: **Left:** Relative error (logarithmic scale) over mesh size at $t = 0.15\,\mathrm{s}$ for $k^F = 10^{-5}\mathrm{m/s}$. **Right:** Top displacement in μm and relative error. The analytical solution is found Figure 5 and equal to -3.772774825 μm.

[4] J. Heywood, R. Rannacher, and S. Turek, International Journal for Numerical Methods in Fluids **22**(5), 325 (Jan. 1996).
[5] S. Turek, J. Hron, M. Madlik, M. Razzaq, H. Wobker, and J. Acker, in H. Bungartz, M. Mehl, and M. Schäfer, eds., *Fluid-Structure Interaction II: Modelling, Simulation, Optimisation* (Springer, 2010), doi 10.1007/978-3-642-14206-2.
[6] http://www.featflow.de